Nuclear Engineering and Technology 51 (2019) 384–393

Contents lists available at ScienceDirect

Nuclear Engineering and Technology

journal homepage: www.elsevier.com/locate/net

Original Article

Experimental validation of a nuclear forensics methodology for source reactor-type discrimination of chemically separated plutonium

Jeremy M. Osborn [a], Kevin J. Glennon [b, c], Evans D. Kitcher [d], Jonathan D. Burns [d], Charles M. Folden III [b, c], Sunil S. Chirayath [a, d, *]

[a] Department of Nuclear Engineering, Texas A&M University, College Station, TX, 77843, USA
[b] Cyclotron Institute, Texas A&M University, College Station, TX, 77843, USA
[c] Department of Chemistry, Texas A&M University, College Station, TX, 77843, USA
[d] Center for Nuclear Security Science & Policy Initiatives, Texas A&M University, College Station, TX, 77843, USA

ARTICLE INFO

Article history:
Received 7 May 2018
Received in revised form
5 November 2018
Accepted 6 November 2018
Available online 10 November 2018

Keywords:
Nuclear forensics
Reactor-type discrimination
Weapons-useable plutonium
Intra-element isotope ratios
Maximum likelihood

ABSTRACT

An experimental validation of a nuclear forensics methodology for the source reactor-type discrimination of separated weapons-useable plutonium is presented. The methodology uses measured values of intra-element isotope ratios of plutonium and fission product contaminants. MCNP radiation transport codes were used for various reactor core modeling and fuel burnup simulations. A reactor-dependent library of intra-element isotope ratio values as a function of burnup and time since irradiation was created from the simulation results. The experimental validation of the methodology was achieved by performing two low-burnup experimental irradiations, resulting in distinct fuel samples containing sub-milligram quantities of weapons-useable plutonium. The irradiated samples were subjected to gamma and mass spectrometry to measure several intra-element isotope ratios. For each reactor in the library, a maximum likelihood calculation was utilized to compare the measured and simulated intra-element isotope ratio values, producing a likelihood value which is proportional to the probability of observing the measured ratio values, given a particular reactor in the library. The measured intra-element isotope ratio values of both irradiated samples and its comparison with the simulation predictions using maximum likelihood analyses are presented. The analyses validate the nuclear forensics methodology developed.

1. Introduction

The 2018 Nuclear Posture Review reiterated that nuclear terrorism remains among the most significant threats to the United States [1]. An aspect of combatting this threat includes technical nuclear forensics and attribution capabilities as a deterrent to state support of nuclear terrorism [1]. This threat regarding nuclear terrorism and weapons-grade plutonium outside of IAEA safeguards led the authors to develop a nuclear forensics methodology, capable of source reactor-type discrimination of separated weapons-useable plutonium [2]. In the event of plutonium interdiction, the developed reactor-type discrimination methodology may be combined with additional forensic evidence to contribute to the source attribution of the plutonium. The developed reactor-type discrimination methodology utilizes a library comparison technique paired with a maximum likelihood calculation in which, a set of measured intra-element isotope ratio values is compared to a library of the same ratio values created through computational models of multiple reactor types. The methodology results in a maximum likelihood value for each reactor in the library. The likelihood value is proportional to the probability of observing the set of measured intra-element isotope ratio values given a particular reactor in the library. The maximum likelihood values are used to identify the reactor within the library that is the most likely source of the measured material. Along with the maximum likelihood value, the methodology provides a prediction for the parameters of fuel burnup and time since irradiation of the material [2]. Multiple methods were utilized to estimate the standard deviation in the maximized log-likelihood, predicted burnup, and predicted time since irradiation values.

The developed reactor-type discrimination methodology has been previously verified utilizing simulation data instead of measured data [2]. The objective of the research presented here is

* Corresponding author.
E-mail address: sunilsc@tamu.edu (S.S. Chirayath).

https://doi.org/10.1016/j.net.2018.11.003

to perform an experimental validation of the developed nuclear forensics methodology. To do so, two experimental irradiation campaigns were performed, resulting in two distinct fuel samples containing weapons-useable plutonium [3,4]. To replicate weapons-useable plutonium produced in the blanket of a fast breeder reactor, depleted uranium dioxide (DUO_2) fuel samples were placed in a gadolinium sheath and irradiated within the High Flux Isotope Reactor (HFIR) at Oak Ridge National Laboratory (ORNL) [3]. As a surrogate for weapons-useable plutonium produced in a natural uranium-fueled thermal reactor, natural uranium dioxide (UO_2) fuel samples were irradiated in a thermal neutron spectrum at the University of Missouri Research Reactor (MURR) [4]. The irradiated samples were subjected to nondestructive and destructive analyses (NDA and DA) at Texas A&M University to measure the plutonium and fission product isotope values from which the set of intra-element isotope ratios required for the nuclear forensics methodology were derived.

Sec. 2 provides a description of the reactor-type discrimination methodology and a description of the reactors currently in the library. Sec. 3 provides a description of the experimental irradiations and subsequent measurements of the HFIR-irradiated and MURR-irradiated fuel samples. The measured intra-element isotope ratio values are presented in Sec. 4, in addition to the maximum likelihood analysis results, for both experimental validation test cases. In Sec. 5, a parametric bootstrap approach is employed to investigate the effects of sampling the measurement values from a normal distribution created based on the measurement values and associated standard deviation. Finally, Sec. 6 provides a summary of the key results and conclusions drawn from the experimental validation campaigns.

2. Description of the nuclear forensics reactor-type discrimination methodology

The novelty of the developed reactor-type discrimination methodology arises from the focus on chemically separated weapons-useable plutonium, and therefore dependence on intra-element isotope ratios as forensic signatures [2]. Traditional nuclear forensics techniques exist which are based on a knowledge of isotopic concentrations in the spent fuel. However, in the event of plutonium interdiction, it is likely that the irradiated material will have undergone an unknown suite of chemical actinide separation processes. As a result, knowledge of the original isotopic concentrations in the spent fuel are lost. Plutonium Uranium Redox Extraction [5] separations performed by the Texas A&M University Nuclear Forensics Group have demonstrated that a measure of the effectiveness of separation, known as a decontamination factor, varies drastically between elements of interest to nuclear forensics and is a strong function of the separation process parameters [6]. As such, predicting an amount of isotope separation would be unrealistic without knowledge of the specific process parameters. To combat this, the authors developed a methodology utilizing intra-element isotope ratios, since isotopes of the same element will exhibit the same behaviors during chemical separation processes. Intra-element isotope ratios will retain their forensic information while being independent of chemical separation technique or efficiency. The set of intra-element isotope ratios utilized in this work consists of the following ten ratios: $^{137}Cs/^{133}Cs$, $^{134}Cs/^{137}Cs$, $^{135}Cs/^{137}Cs$, $^{154}Eu/^{153}Eu$, $^{136}Ba/^{138}Ba$, $^{150}Sm/^{149}Sm$, $^{152}Sm/^{149}Sm$, $^{240}Pu/^{239}Pu$, $^{241}Pu/^{239}Pu$, and $^{242}Pu/^{239}Pu$. A description on the contribution of each intra-element isotope ratio to resolving the parameters of burnup, time since irradiation, and reactor-type can be found in Osborn et al. [2].

2.1. Maximum likelihood calculation as a characterization method

The developed reactor-type discrimination methodology utilizes a library comparison approach coupled with a maximum likelihood calculation. Computational fuel burnup simulations were performed for multiple reactor types to create a reactor-dependent library of values for the intra-element isotope ratios of interest as a function of fuel burnup and time since irradiation. The maximum likelihood calculation utilizes the product of probability density functions to calculate the likelihood that a measured set of intra-element isotope ratio values could be produced from a given reactor model within the library. The largest likelihood value will be indicative of the most likely reactor model, burnup, and time since irradiation which corresponds to the set of simulated intra-element isotope ratio values that most closely matches the set of measured intra-element isotope ratio values. The log-likelihood is the natural logarithm of the likelihood equation. By using the log-likelihood computational overflow errors were avoided in the calculation. The likelihood [7] and log-likelihood of reactor model, M, matching the measured set of intra-element ratios, r_{mes}, are given by the following equations:

$$L(M|r_{mes}) \propto f(r_{mes}|M) = \prod_{j=1}^{n} \frac{1}{\sigma_{j,sim}\sqrt{2\pi}} exp\left\{ -\frac{(r_{j,mes} - r_{j,sim})^2}{2\sigma_{j,sim}^2} \right\} \tag{1}$$

$$Log\ L(M|r_{mes}) = \sum_{j=1}^{n} \left[log\left(\frac{1}{\sigma_{j,sim}\sqrt{2\pi}} \right) - \frac{(r_{j,mes} - r_{j,sim})^2}{2\sigma_{j,sim}^2} \right] \tag{2}$$

where, $r_{j,mes}$ is the jth intra-element isotope ratio (for example $^{137}Cs/^{133}Cs$) in a set of n measured intra-element ratios, $r_{j,sim}$ is the jth intra-element isotope ratio in a set of n simulated intra-element ratios from model, M, and $\sigma_{j,sim}$ is the simulation error standard deviation associated with the jth intra-element ratio value from the set, r_{sim}. By using the propagation of errors, the variance in the log-likelihood is approximated by the following equation:

$$\sigma_{Log\ L}^2 \cong \sum_{j=1}^{n} \left(\frac{(r_{j,mes} - r_{j,sim})}{\sigma_{j,sim}^2} \right)^2 \times \left(\sigma_{j,mes}^2 + \sigma_{j,sim}^2 \right) \tag{3}$$

where, $\sigma_{j,mes}$ is the measurement error standard deviation associated with the jth intra-element ratio value from the set, r_{mes}. The approximation for the standard deviation in the log-likelihood resulting from Eq. (3), can be used to assess confidence in the identified reactor model.

The logarithm is a strictly increasing function. Thus, the set of simulated intra-element isotope ratio values which maximizes the likelihood will also maximize the log-likelihood. The likelihood value will be used for visualization, whereas the log-likelihood value and approximate standard deviation in the log-likelihood will be used to identify the most likely reactor model that could have produced the measured material.

2.2. Reactor library and modeling

Each reactor model contained in the reactor library was developed and simulations were performed using one of two versions of the Monte Carlo radiation transport codes, MCNPX Version 2.7 [8] and MCNP6 [9]. Both versions of the MCNP code track material

burnup via the integrated CINDER-90 [10] module. Reactor core physics and fuel irradiation were simulated to a burnup of approximately 5 GWd/MTU, and used to generate the intra-element isotope ratio values in the irradiated fuel as a function of burnup. For isotopes having short-lived precursors, at each burn step the short-lived precursors were summed with the isotope of interest. This allows the ratio values, as a function of burnup, to be representative of a measured value at a later measurement date. The MCNP simulations utilized reactor-appropriate burnup time steps to sufficiently capture isotope generation and depletion. The intra-element isotope ratios were then expanded to 500 burnup time steps using linear interpolation for storage in the library. Appropriate decay equations were used to calculate the intra-element isotope ratio values from each burnup time step as a function of time since irradiation ended ranging from 0 to 5000 days in 1-day intervals. Consequently, for each reactor model, the reactor-dependent library consists of a 500 burnup step x 5000 time since irradiation step matrix containing values for the set of intra-element isotope ratio values.

Currently, the reactor library consists of nine reactor models; two of which are the simulations of the experimental irradiations performed at HFIR and MURR for the validation of the nuclear forensics methodology presented in this paper. The HFIR core was developed by ORNL for reactor cycle 400 [11] and provided as part of support for the experimental irradiation. The model was modified to include the DUO_2 fuel discs and gadolinium capsule in the irradiation location. The HFIR model was used to produce best estimate values for the material isotopics at the end of the experimental irradiation. Additionally, the HFIR model simulation was extended past the known irradiation to a burnup of approximately 5 GWd/MTU for consistency within the reactor library. Details of the experimental irradiation at HFIR can be found in Swinney et al. [3]. The MURR core was developed based on reactor characteristics found in the 2006 MURR Safety Analysis Report (SAR) [12]. Information on the irradiation location and a detailed irradiation history was provided by MURR staff. The MURR model was used to produce best estimate values for the material isotopics at the end of the experimental irradiation. Additionally, the MURR model simulation was extended past the known irradiation to a burnup of approximately 5 GWd/MTU for consistency within the reactor library. Details of the experimental irradiation at MURR can be found in Osborn et al. [4]. The HFIR and MURR models contained in the reactor library are not indicative of the HFIR and MURR reactor cores, but rather the sample material irradiation which took place within each reactor facility.

The other reactors in the library are a pressurized water reactor (PWR) at three enrichments, the blanket material of a fast breeder reactor (FBR), a pressurized heavy water reactor (PHWR), a Magnox reactor, and an NRX reactor. The AP1000 was modeled to represent the PWR [2,13]. PWR burnup simulations were performed for fuel assemblies at enrichments of 2.35 wt%, 3.4 wt%, and 4.45 wt% ^{235}U. Characteristics of the FBR modeled for this study are available in open literature [14–16]. FBR burnup simulations were performed for the DUO_2 radial blanket where low-burnup plutonium is produced. The PHWR, NRX and Magnox reactors are all thermal neutron reactors fueled with natural uranium [17,18]. The PHWR modeled was an Indian 220-MWe PHWR [4,19], the NRX modeled was Iran's IR-40 [4,20,21], and the Magnox core modeled was the North Korean Yongbyon reactor [4,22,23]. Table 1 contains some key parameters of the reactor cores modeled. Table 2 contains the neutron flux calculated within the fuel region of interest for each model at the beginning of the MCNP burnup simulations. The relative stochastic error on the neutron flux magnitude was less than 1% for each simulation.

3. Experimental irradiation campaigns and associated measurements

3.1. Experimental irradiation campaigns

The nuclear forensics reactor-type discrimination methodology was previously verified utilizing simulation data rather than measurement data [2]. To allow for experimental validation of the developed methodology, two irradiation campaigns were performed, resulting in two distinct fuel samples containing weapons-useable plutonium. For the DUO_2 fuel disc samples irradiated at HFIR and the natural UO_2 fuel disc samples irradiated at MURR, following irradiation a single disc was chosen and dissolved in 8 M nitric acid (HNO_3) to produce a solution. Aliquots of each solution were analyzed using gamma and mass spectrometry in order to characterize the irradiated materials through measurements of plutonium and fission product isotopes [3,4].

3.1.1. Experimental irradiation at HFIR

In 2013, an irradiation was performed for the purpose of producing sample material consistent with the plutonium produced within the low-burnup DUO_2 blanket material of a fast breeder reactor [3]. The experimental irradiation consisted of DUO_2 fuel discs burned to a low burnup in the HFIR core. The HFIR is a thermal neutron reactor, thus a pseudo-fast neutron flux was achieved by placing the DUO_2 discs within a gadolinium (Gd) sheath inside of the aluminum irradiation capsule. The intended burnup was approximately 1 GWd/MTU. However, the discs were unintentionally irradiated to a higher burnup. Investigations presented here indicate that after approximately 1 GWd/MTU of burnup, depletion of the Gd sheath inside the irradiation capsule resulted in the DUO_2 discs being subsequently irradiated in a thermal neutron spectrum. The varying neutron flux for the experimental irradiation at HFIR is discussed in more detail in Sec. 4.3.1.

Following completion of the experimental irradiation at HFIR on June 1, 2013, one of the 12.9 mg DUO_2 fuel discs was dissolved in 8 M nitric acid and was characterized through gamma and mass spectrometry of the solution. Results from the characterization concluded that the DUO_2 fuel discs were irradiated to a burnup of 4.36 ± 0.28 GWd/MTU, and the irradiation produced nearly 200 μg of plutonium with 89% ^{239}Pu [3]. For the interested reader, a full description of the DUO_2 fuel sample irradiation in HFIR, and subsequent measurements can be found in Swinney et al. [3].

3.1.2. Experimental irradiation at MURR

In 2016, a second experimental irradiation was conducted for the purpose of producing sample material consistent with the plutonium produced within a natural uranium fueled thermal reactor. The irradiation consisted of natural UO_2 fuel discs burned to a low burnup in a thermal neutron spectrum at the MURR facility [4]. The MURR is a highly-enriched uranium (HEU) fueled, light water cooled reactor core surrounded by beryllium and graphite reflectors. The graphite reflector surrounding the MURR core was designed to allow for large sample irradiations, and housed the natural UO_2 fuel samples during irradiation.

Following completion of the experimental irradiation at MURR on April 25, 2017, one of the 16.46 mg natural UO_2 fuel discs was dissolved in 8 M nitric acid and was characterized through gamma and mass spectrometry of the solution. Results from the forensic characterization concluded that the natural UO_2 fuel discs were irradiated to a burnup of 0.97 ± 0.03 GWd/MTU, and the irradiation produced approximately 20 μg of plutonium with 95% ^{239}Pu [4]. For the interested reader, a full description of the natural UO_2 fuel sample irradiation in MURR, and subsequent measurements can be found in Osborn et al. [4].

Table 1
Reactor library model characteristics [11–15,19–23].

Reactor Model	Thermal Power (MWth)	Fuel Type (at.%^{235}U)	Moderator	Coolant
PWR (2.35%)[a]	3400	UO_2 (2.35)	Light Water	Light Water
PWR (3.4%)[a]	3400	UO_2 (3.4)	Light Water	Light Water
PWR (4.45%)[a]	3400	UO_2 (4.45)	Light Water	Light Water
FBR	1250	UO_2 (0.25)[b]	–	Liquid Sodium
PHWR	756	UO_2 (0.72)	Heavy Water	Heavy Water
NRX	40	UO_2 (0.72)	Heavy Water	Heavy Water
Magnox	25	U metal w/0.5% Al (0.72)	Graphite	Carbon Dioxide
HFIR	85	UO_2 (0.25)[c]	Light Water	Light Water
MURR	10	UO_2 (0.72)[d]	Light Water, Beryllium, Graphite	Light Water

[a] The PWR model has fuel assemblies at three different enrichments (2.35%, 3.4%, and 4.45%^{235}U enrichment).
[b] The FBR has a MOX core and depleted UO_2 blanket region. The material analyzed here is from the FBR radial blanket region.
[c] The HFIR model is not indicative of the HEU-fueled HFIR core. Rather, the HFIR model is a simulation of the experimental irradiation at HFIR plus an extension to a burnup of approximately 5 GWd/MTU.
[d] The MURR model is not indicative of the HEU-fueled MURR core. Rather, the MURR model is a simulation of the experimental irradiation at MURR plus an extension to a burnup of approximately 5 GWd/MTU.

Table 2
MCNP calculated neutron flux at the beginning of burn for the library reactor models.

Reactor Model	Total Flux (n/cm^2-s)	Thermal Flux E < 0.5 eV (n/cm^2-s)	Fast Flux E > 0.1 MeV (n/cm^2-s)
PWR (2.35%)	4.09×10^{14}	7.09×10^{13}	1.86×10^{14}
PWR (3.4%)	3.47×10^{14}	4.45×10^{13}	1.66×10^{14}
PWR (4.45%)	1.74×10^{14}	2.01×10^{13}	8.68×10^{13}
FBR	5.79×10^{14}	6.50×10^{9}	2.17×10^{14}
PHWR	1.75×10^{14}	6.04×10^{13}	6.51×10^{13}
NRX	3.27×10^{13}	1.58×10^{13}	9.83×10^{12}
Magnox	8.30×10^{12}	3.32×10^{12}	2.67×10^{12}
HFIR	1.60×10^{15}	5.86×10^{12}	8.03×10^{14}
MURR	5.06×10^{13}	3.15×10^{13}	4.62×10^{12}

3.2. Intra-element isotope ratio measurements

In support of the study presented here, an additional set of gamma and mass spectrometry measurements were performed on both irradiated fuel samples in order to obtain measured values for the intra-element isotope ratios utilized in the maximum likelihood analysis.

Gamma spectrometry was performed at Texas A&M University using a Canberra Standard Electrode Coaxial HPGe detector within a lead shielded cave. Prior to each measurement, an energy and efficiency calibration was conducted with a NIST traceable liquid ^{152}Eu source. Gamma spectrometry was used to measure the ^{134}Cs/^{137}Cs ratio within both HFIR and MURR samples, as well as the amount of ^{154}Eu for calculating the ^{154}Eu/^{153}Eu ratio in the HFIR irradiated material.

Multiple aliquots of both irradiated fuel sample solutions were prepared, and inductively coupled plasma mass spectrometry (ICP-MS) was performed using a Thermo Fisher Scientific iCAP RQ spectrometer at Texas A&M University. Calibration standards were prepared for Cs, Ce, Sm, Eu, and U at concentrations from 0.01 ppb to 500 ppb using 1000 ppm ICP-MS standards purchased from BDH Chemicals. The uranium calibration was used to calculate the percentage of ^{238}U hydride (UH+) formation. When measuring the sample aliquots, the percentage of UH + formation was used to correct the 239 amu mass bin to the contribution from ^{239}Pu. Individual aliquots were measured 90 times to calculate an average and standard deviation of each mass-to-charge ratio bin per aliquot. The measurement errors calculated are the relative standard deviation (RSD) of the measured mass ratios. The measurement standard deviations were calculated by fully propagating the standard deviations of the individual measurements and contain standard deviations from the calibration curve, standard deviations from the mass spectrometry measurements, and random errors in pipetting.

Isobaric interferences must be considered when utilizing mass spectrometry to measure the isotopics of a sample. Of the isotope ratios measured via mass spectrometry, four isobaric interferences were identified and addressed. Mass 137 amu consisted of ^{137}Cs and its decay product, ^{137}Ba. Mass 150 amu consisted of ^{150}Sm and ^{150}Nd. Mass 154 amu contained primarily ^{154}Sm with ^{154}Eu and ^{154}Gd. Lastly, mass 241 amu consisted of ^{241}Pu and ^{241}Am. For long decay times, the isobaric interference between ^{135}Cs and its decay product, ^{135}Ba, may need to be considered, however for the decay times encountered here the 135 amu mass is entirely ^{135}Cs due to the long half-life of ^{135}Cs. Two techniques were used to address the isobaric interferences. The first technique was application of a fissiogenic ratio [3,4] based on the MCNP simulation results to delineate the contribution of a desired isotope to a mass spectrometry measured isobar. The second technique was to perform a chemical separation of the element of interest prior to measurement by mass spectrometry. Theoretically a chemical separation technique could be used to isolate each element containing an isobaric isotope. This chemical separation approach was employed to measure the ^{150}Sm/^{149}Sm ratio while avoiding the ^{150}Sm and ^{150}Nd isobaric interference. Cation exchange column chromatography has the ability to separate the lanthanide elements due to lanthanide contraction [24]. Column chromatography employing a Dowex-50W X4 200–400 mesh resin and an α–HIB eluent was used to separate Sm from Nd. Chromatography was performed on the benchtop using a 3.1 mm inner diameter glass column with a bed height of 210 mm. The mobile phase was prepared as 0.4 M α-HIB at pH 3.00, and the resin was rinsed and converted to the NH4+ form prior to use. Fractions from the column were collected each free column volume and measured individually via ICP-MS after

dilution with 1% HNO_3. The $^{150}Sm/^{149}Sm$ ratio was determined within the Sm elution peak, which contained no ^{150}Nd, by mass spectrometry. Results from these measurements are presented in Sec. 4.

3.2.1. HFIR irradiated material measurements

On October 19, 2017 gamma and mass spectrometry of the HFIR-irradiated DUO_2 material was performed in order to obtain measured values for the intra-element isotope ratios. Four aliquots with 0.04% of the dissolved HFIR irradiated disc were prepared for mass spectrometry by dilution into 5 mL of ultra-pure 1% HNO_3. Barium contamination in the mass spectrometry data from barium present in the mass spectrometer tuning solution rendered the $^{136}Ba/^{138}Ba$ ratio unusable. As a result, only nine of the ten intra-element isotope ratios were employed for the HFIR analysis.

The 154 amu mass bin was dominated by ^{154}Sm, and thus the gamma spectrometry measured concentration of ^{154}Eu was used for the $^{154}Eu/^{153}Eu$ ratio. In order to ratio the gamma spectrometry measured ^{154}Eu and mass spectrometry measured ^{153}Eu, the concentration of ^{153}Eu to uranium had to be determined. An additional aliquot containing 0.0004% of the dissolved disc was measured to quantify the mass of uranium. The concentration of uranium in the 0.0004% aliquot was used to determine the concentration of uranium in each of the 0.04% aliquots, such that the ^{153}Eu could be normalized to uranium. All other mass spectrometry measured ratios use the average measurements from the four 0.04% aliquots, without normalizing to uranium. Table 3 provides the measurement technique used as well as additional comments on the method used to account for any mass spectrometry interferences of the nine measured intra-element isotope ratios from the HFIR irradiated material.

4. . MURR irradiated material measurements

On March 9, 2018 gamma and mass spectrometry of the MURR-irradiated natural UO_2 material was performed in order to obtain measured values for the intra-element isotope ratios. Three aliquots with 1% of the dissolved MURR irradiated disc were prepared for mass spectrometry by dilution into 5 mL of ultra-pure 1% HNO_3. Again, barium contamination in the mass spectrometer tuning solution rendered the $^{136}Ba/^{138}Ba$ ratio unusable. Additionally, a measured value for the $^{154}Eu/^{153}Eu$ ratio was not obtained due to the amount of ^{154}Eu in the MURR sample being below the minimum detectable limit via mass spectrometry or gamma spectrometry. Thus, the eight measured intra-element ratios from the MURR irradiated material are contained in Table 4 with the measurement technique used and additional comments on the method to account for any interferences which occurred in mass spectrometry.

5. Results and discussion

5.1. Measured intra-element isotope ratio values

Table 5 contains the nine measured intra-element ratio values for the HFIR irradiated material, and Table 6 contains the eight measured intra-element ratio values for the MURR irradiated material. The measurement error standard deviations are also included in Tables 5 and 6 in the form of relative standard deviation.

5.2. Maximum likelihood analysis results

5.2.1. HFIR irradiated material maximum likelihood analysis

Using the measured set of nine intra-element ratio values contained in Table 5, the maximum likelihood analysis was performed using equations (1)–(3) for the DUO_2 fuel samples experimentally irradiated at HFIR. Table 7 contains the results of the maximum likelihood analysis on the HFIR irradiated material. Each library reactor model is ranked based on the log-likelihood value. Also tabulated is the predicted fuel burnup and time since irradiation corresponding to the maximum log-likelihood value. From Eq. (2) it is evident that the maximum possible log-likelihood value, for a given measurement, will occur when the set of measured intra-element isotope ratio values perfectly matches with a simulation set. Thus, the maximum possible log-likelihood value is a function of the simulation error standard deviation, $\sigma_{j,sim,}$ if and when the simulation set is equal to the measurement set, $r_{sim} = r_{mes}$. Currently, MCNP does not have the ability to propagate the standard deviation in isotope concentrations through burnup simulations. Previous post irradiation examination studies have shown that errors of up to 10% can be expected for MCNP predictions of actinides and fission products [3,4]. Thus, a 10% relative standard deviation was assumed for the error in the simulated concentration of each isotope. Propagated together, a relative standard deviation of approximately 14% was assumed as the error for each simulated ratio value. With the assumed relative standard deviation on the simulation ratio value and the condition $r_{sim} = r_{mes,}$ Eq. (2) calculated the maximum possible log-likelihood (a perfect match) value for the HFIR irradiated material as 28.7.

Table 7 shows that the reactor-type discrimination methodology correctly identified the most likely source reactor model for the measured material as the HFIR model, with a log-likelihood value of 17.7 ± 5.0 compared to a maximum possible log-likelihood value of 28.7. The predicted burnup and time since irradiation for the HFIR model corresponding with the maximum log-likelihood value is 4.29 GWd/MTU and 1833 days, respectively, compared to the known burnup of 4.36 ± 0.28 GWd/MTU and decay of 1601 days. The predicted burnup and time since irradiation are within 2% and 15% of the known values, respectively. The resulting 3-dimensional likelihood surface map and 2-dimensional likelihood contour map

Table 3
HFIR irradiated material intra-element isotope ratio measurement technique and comments.

Ratio	Additional Comments on Measurement Interferences
$^{137}Cs/^{133}Cs$[a]	Fissiogenic ratio of 0.902 applied to ^{137}Cs
$^{134}Cs/^{137}Cs$[b]	No interference
$^{135}Cs/^{137}Cs$[a]	Fissiogenic ratio of 0.902 applied to ^{137}Cs
$^{154}Eu/^{153}Eu$ [a,b]	No interference
$^{150}Sm/^{149}Sm$[a]	Column chromatography separation of Sm
$^{152}Sm/^{149}Sm$[a]	No interference
$^{240}Pu/^{239}Pu$[a]	UH + formation corrected ^{239}Pu
$^{241}Pu/^{239}Pu$[a]	Fissiogenic ratio of 0.810 applied to ^{241}Am, UH + formation corrected ^{239}Pu
$^{242}Pu/^{239}Pu$[a]	UH + formation corrected ^{239}Pu

[a] Measured via mass spectrometry.
[b] Measured via gamma spectrometry.

Table 4
MURR irradiated material intra-element isotope ratio measurement technique and comment.

Ratio	Additional Comments on Measurement Interferences
$^{137}Cs/^{133}Cs$[a]	Fissiogenic ratio of 0.976 applied to ^{137}Cs
$^{134}Cs/^{137}Cs$[b]	No interference
$^{135}Cs/^{137}Cs$[a]	Fissiogenic ratio of 0.976 applied to ^{137}Cs
$^{150}Sm/^{149}Sm$[a]	Column chromatography separation of Sm
$^{152}Sm/^{149}Sm$[a]	No interference
$^{240}Pu/^{239}Pu$[a]	UH + formation corrected ^{239}Pu
$^{241}Pu/^{239}Pu$[a]	Fissiogenic ratio of 0.955 applied to ^{241}Am, UH + formation corrected ^{239}Pu
$^{242}Pu/^{239}Pu$[a]	UH + formation corrected ^{239}Pu

[a] Measured via mass spectrometry.
[b] Measured via gamma spectrometry.

Table 5
Measured intra-element isotope ratio values for the HFIR irradiated material.

Ratio	Measured Value	Measurement Error (%RSD)
$^{137}Cs/^{133}Cs$	1.30×10^{0}	6.7
$^{134}Cs/^{137}Cs$	3.74×10^{-3}	4.2
$^{135}Cs/^{137}Cs$	4.25×10^{-1}	10
$^{154}Eu/^{153}Eu$	4.67×10^{-2}	4.5
$^{150}Sm/^{149}Sm$	3.23×10^{0}	2.7
$^{152}Sm/^{149}Sm$	2.93×10^{0}	1.3
$^{240}Pu/^{239}Pu$	8.28×10^{-2}	0.6
$^{241}Pu/^{239}Pu$	2.67×10^{-2}	0.9
$^{242}Pu/^{239}Pu$	1.88×10^{-3}	0.9

Table 6
Measured intra-element isotope ratio values for the MURR irradiated material.

Ratio	Measured Value	Measurement Error (%RSD)
$^{137}Cs/^{133}Cs$	9.75×10^{-1}	6.6
$^{134}Cs/^{137}Cs$	3.84×10^{-3}	7.0
$^{135}Cs/^{137}Cs$	2.95×10^{-1}	6.8
$^{150}Sm/^{149}Sm$	9.88×10^{0}	6.7
$^{152}Sm/^{149}Sm$	6.65×10^{0}	5.7
$^{240}Pu/^{239}Pu$	4.77×10^{-2}	5.7
$^{241}Pu/^{239}Pu$	2.29×10^{-3}	5.8
$^{242}Pu/^{239}Pu$	5.99×10^{-5}	8.3

for the HFIR model (the most likely reactor model in this case) are illustrated in Fig. 1(a) and (b), respectively.

The next most likely reactor models are the MURR, NRX, and Magnox models. This is a non-intuitive result as these three models are thermal neutron irradiations. For the MURR and NRX models, the log-likelihood value is poor while the burnup and time since irradiation predictions are fairly good. This is due to the similarity between the selected set of simulated intra-element ratio values and the set of measured intra-element ratio values which contribute to burnup and time since irradiation predictions, but dissimilar values for the $^{135}Cs/^{137}Cs$, $^{150}Sm/^{149}Sm$, and $^{152}Sm/^{149}Sm$ ratios which depend heavily on thermal neutron flux magnitude and largely contribute to the reactor-type prediction. It should be noted that for the FBR and all three PWR models, the predicted burnup occurs at the maximum burnup level simulated for the respective models. Therefore, a prediction of this value is interpreted as the most likely point occurring at, or beyond, the boundary of the simulated burnup space.

Based on the maximum likelihood analysis the FBR model is the least likely source of the HFIR irradiated material. Again, this is a non-intuitive result as the experimental irradiation at HFIR was intended to serve as a surrogate to FBR blanket material. The Gd-lined irradiation capsule was utilized to absorb the thermal component of the HFIR neutron flux. However, depletion of neutron-absorbing isotopes of Gd (^{152}Gd, ^{155}Gd, and ^{157}Gd) occurred throughout the irradiation. As a result of the depletion of the Gd capsule, the fuel discs were exposed to the full (thermal) HFIR neutron flux for the majority of the irradiation after 1 GWd/MTU of burnup was surpassed. Fig. 2 displays the 238-energy-group neutron flux, as calculated by MCNP, observed by the DUO_2 fuel discs at the beginning of irradiation and end of irradiation, as well as for the FBR radial blanket. This shows that the flux at the beginning of the HFIR irradiation contained a significant epi-thermal contribution which is not present in an actual FBR blanket neutron flux, and moved even further to a thermal flux throughout the irradiation. For simplicity, the HFIR flux at only the beginning and end of irradiation is plotted, however the MCNP simulation showed the flux spectra gradually became more thermal throughout the irradiation. Table 8 contains the values of the neutron flux magnitude exposed to the DUO_2 fuel discs at the beginning and end of irradiation at HFIR, indicating that the total neutron flux increased by nearly 50% and the thermal neutron flux increased by more than two orders of magnitude. In terms of neutron fluence, which is the time integral of the neutron flux, the DUO_2 fuel discs were exposed to a larger thermal neutron fluence than a fast/epi-thermal neutron fluence. The HFIR model

Table 7
Results of maximum likelihood analysis for the HFIR irradiated material.[a]

Reactor Model	Log-Likelihood Value[b]	Predicted Burnup (GWd/MTU)	Predicted Time Since Irradiation (days)
HFIR	$+17.7 \pm 5.0$	4.29	1833
MURR	-38.9 ± 12.2	3.76	1647
NRX	-43.5 ± 11.8	3.71	1524
Magnox	-51.4 ± 12.7	2.79	491
PWR (2.35%)	-70.6 ± 19.4	$\geq$5.31	1861
PHWR	-131 ± 35	3.31	2022
PWR (3.4%)	-279 ± 26	$\geq$5.01	792
PWR (4.45%)	$(-5.50 \pm 0.14) \times 10^{3}$	$\geq$3.90	0
FBR	$(-6.26 \pm 0.10) \times 10^{5}$	$\geq$4.73	0

[a] Measured material was HFIR irradiated to a burnup of 4.36 ± 0.28 GWd/MTU with 1601 days of time since irradiation.
[b] The maximum possible log-likelihood value for the measurement set was 28.7.

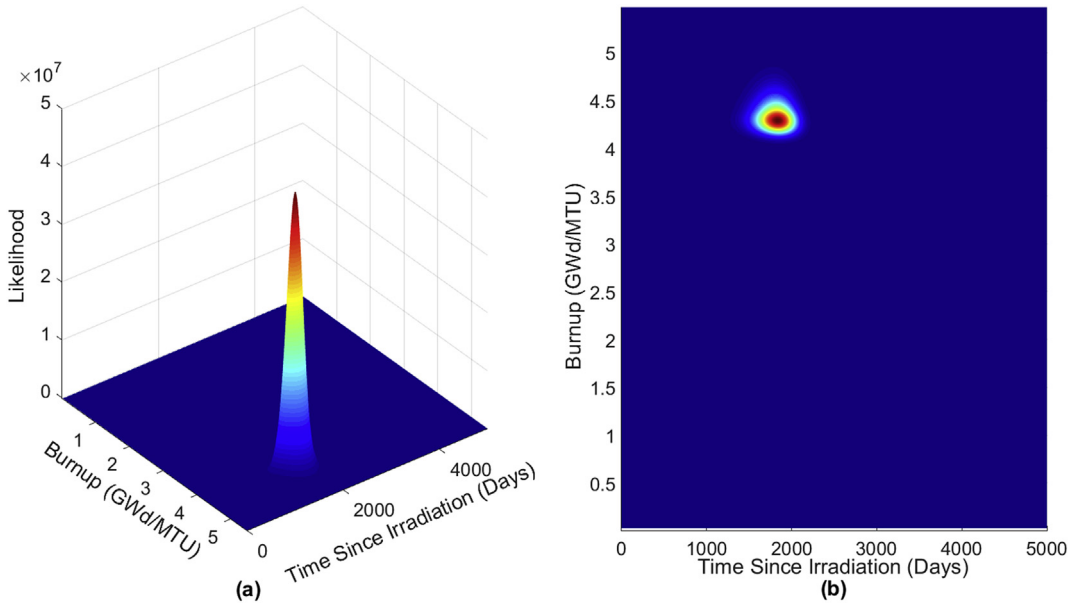

Fig. 1. Results of maximum likelihood analysis for the HFIR irradiated material (a) 3-D likelihood surface map and (b) 2-D contour map for the most likely reactor (HFIR).

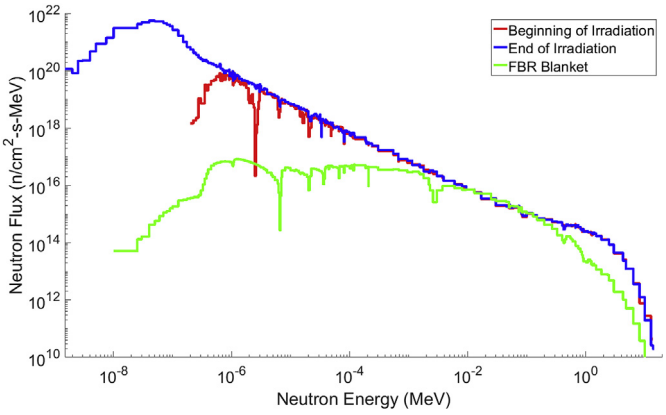

Fig. 2. The MCNP calculated 238-energy-group neutron flux per MeV for the experimental irradiation at HFIR at the beginning of irradiation and the end of irradiation, due to the depletion of the gadolinium irradiation capsule, compared to that of the FBR blanket.

simulating the experimental irradiation at HFIR includes the behavior of the Gd irradiation capsule depletion and changing neutron flux.

5.2.2. *MURR irradiated material maximum likelihood analysis*

Using the measured set of eight intra-element ratio values contained in Table 6, the maximum likelihood analysis was performed using equations (1)–(3) for the natural UO_2 fuel samples experimentally irradiated at MURR. Table 9 contains the results of the maximum likelihood analysis on the MURR irradiated material. Each library reactor model is ranked based on the log-likelihood value. As before, the predicted fuel burnup and time since irradiation corresponding to the largest log-likelihood value is also tabulated. The maximum possible log-likelihood value for the MURR irradiated material was calculated as 29.8.

Table 9 shows that the reactor-type discrimination methodology correctly identified the most likely source reactor model for the measured material as the MURR model, with a log-likelihood value of 29.5 ± 1.1 compared to a maximum possible log-likelihood value of 29.8. The predicted burnup and time since irradiation for the MURR model corresponding with the maximum log-likelihood value is 1.01 GWd/MTU and 303 days, respectively, compared to the known burnup of 0.97 ± 0.03 GWd/MTU and decay of 318 days. The predicted burnup and time since irradiation are within 4% and 5% of the known values, respectively. The resulting 3-dimensional likelihood surface map and 2-dimensional likelihood contour map for the MURR model (the most likely reactor model in this case) are illustrated in Fig. 3(a) and (b), respectively.

Analyzing the log-likelihood values in Table 9 the reactor models can be categorized into groups. The most likely reactor models are the MURR simulation, the NRX, and the Magnox. These results are as expected since the NRX and Magnox are natural uranium fueled thermal reactors, similar to the experimental irradiation at MURR. The PHWR model and three PWR models are grouped together with intermediately low log-likelihood values. It is also evident from the log-likelihood values that neither the fast neutron, FBR model, nor the mixed pseudo-fast to thermal neutron, HFIR model, is the source of the measured material. The maximum likelihood analysis works well for identifying the most likely source reactor model, as well as discriminating against the reactor models which are highly unlikely to be the source reactor type. For the reactor models with intermediately low log-likelihood values, the correct interpretation of the results is that these reactors are not the likely source of the material if operated as modeled. Drawing any

Table 8
Comparison of the MCNP calculated neutron flux magnitude at the beginning and end of the experimental irradiation at HFIR.

HFIR Irradiation	Total Flux Magnitude (n/cm^2-s)	Thermal Flux E < 0.5 eV (n/cm^2-s)	Fast Flux E > 0.1 MeV (n/cm^2-s)
Beginning of Irradiation	1.60×10^{15}	5.86×10^{12}	8.03×10^{14}
End of Irradiation	2.36×10^{15}	6.39×10^{14}	8.05×10^{14}

Table 9
Results of maximum likelihood analysis for the MURR irradiated material.[a]

Reactor Model	Log-Likelihood Value[b]	Predicted Burnup (GWd/MTU)	Predicted Time Since Irradiation (days)
MURR	+29.5 ± 1.1	1.01	303
NRX	+25.6 ± 3.0	1.02	203
Magnox	+13.0 ± 5.7	0.73	0
PWR (3.4%)	−5.97 ± 8.73	3.89	1371
PWR (4.45%)	−9.10 ± 10.3	≥3.90	1195
PWR (2.35%)	−10.4 ± 9.8	3.04	1162
PHWR	−23.5 ± 15.1	0.94	260
HFIR	−167 ± 28	4.40	1788
FBR	(-1.52 ± 0.20) × 10^5	≥4.73	0

[a] Measured material was MURR irradiated to a burnup of 0.97 ± 0.03 GWd/MTU with 318 days of time since irradiation.
[b] The maximum possible log-likelihood value for the measurement set was 29.8.

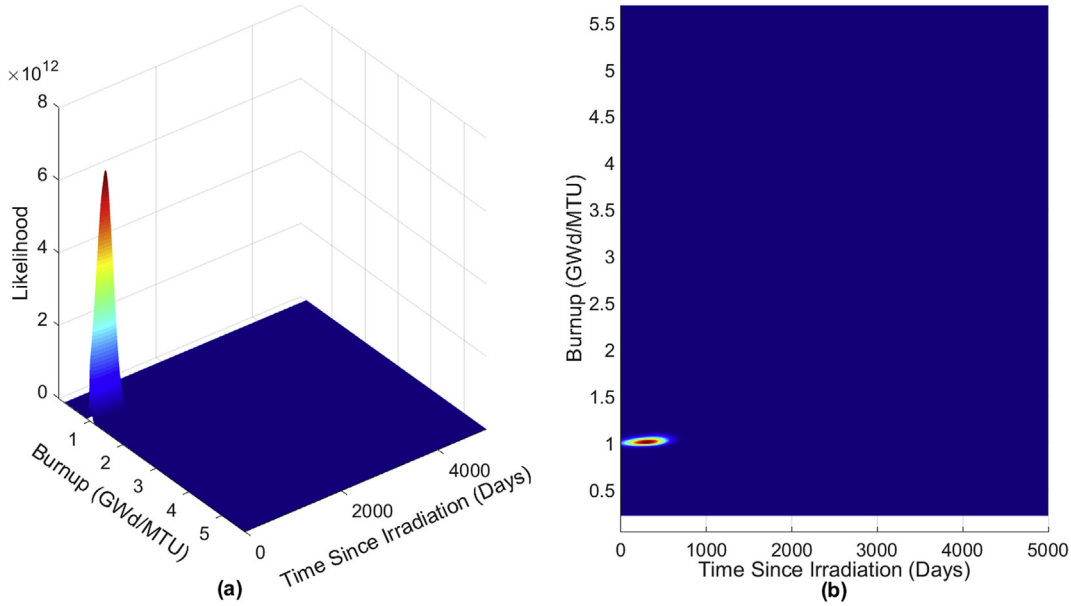

Fig. 3. Results of maximum likelihood analysis for the MURR irradiated material (a) 3-D likelihood surface map and (b) 2-D contour map for the most likely reactor (MURR).

further conclusions from reactor models with low log-likelihood values may not be appropriate.

6. Maximum log-likelihood and predicted parameter sensitivity to measurement standard deviation

Eq. (3) allows an approximate estimation of the variance in the log-likelihood values to be obtained. However, in order to estimate the approximate variance in the predicted parameters of burnup and time since irradiation at the maximized log-likelihood location, a parametric bootstrap approach [25] must be employed on the measured isotope values. The parametric bootstrap was performed by repeated random sampling of the normal distributions created by using the individually measured isotope values and associated measurement standard deviation, then forming the measurement ratios from the sampled isotope values. In doing so, the situation of having multiple measurement values was approximated and the variance estimated. Each measured intra-element ratio value is randomly sampled 250 times and used to perform 250 maximum log-likelihood calculation producing 250 predicted burnup and predicted time since irradiation values. The calculated average and standard deviation values for the maximum log-likelihood, predicted burnup, and predicted time since irradiation are presented in Table 10 and Table 11 for the HFIR irradiated material and MURR irradiated material, respectively.

It should be noted that the results of the parametric bootstrap approach are congruent with the approach utilizing Eq. (3). For both the HFIR and MURR irradiated materials, the estimate of the variance in the log-likelihood values for every model in the reactor library is indeed smaller than the estimate obtained using Eq. (3). This supports the use of the maximum log-likelihood calculated by Eq. (2) and associated approximate standard deviation calculated by Eq. (3). Furthermore, the parametric bootstrap method has produced an estimate of variance in the predicted reactor model parameters. This allows for a range of predicted burnup and predicted time since irradiation values.

For the reactor models with maximum log-likelihood values located at the edge of the simulated burnup space, the parametric bootstrap approach results in very small values for the standard deviation in the burnup predictions as a result of the maximum being located on the edge of the simulated parameter space.

7. Conclusions

Previous research developed and verified a nuclear forensics methodology capable of source reactor-type discrimination of materials containing weapons-grade plutonium, even if the plutonium has been purified and separated [2]. The work presented here provides an experimental validation of the developed nuclear forensics methodology. The experimental validation was

Table 10
Results of 250 realizations of the parametric bootstrap for the HFIR irradiated material.

Reactor Model	Maximum Log-Likelihood Value	Predicted Burnup (GWd/MTU)	Predicted Time Since Irradiation (days)
HFIR	$+17.4 \pm 2.3$	4.29 ± 0.01	1834 ± 54
MURR	-39.8 ± 3.4	3.76 ± 0.03	1648 ± 67
NRX	-44.0 ± 2.3	3.71 ± 0.03	1526 ± 64
Magnox	-51.5 ± 4.1	2.79 ± 0.02	490 ± 60
PWR (2.35%)	-72.4 ± 12.2	$\geq 5.31 \pm < 0.01$	1863 ± 76
PHWR	-135 ± 29	3.34 ± 0.12	2035 ± 122
PWR (3.4%)	-278 ± 7	$\geq 5.01 \pm < 0.01$	741 ± 257
PWR (4.45%)	$(-5.47 \pm 0.10) \times 10^3$	$\geq 3.90 \pm < 0.01$	0 ± 0
FBR	$(-6.23 \pm 0.11) \times 10^5$	$\geq 4.73 \pm < 0.01$	0 ± 0

Table 11
Results 250 realizations of the parametric bootstrap for the MURR irradiated material.

Reactor Model	Maximum Log-Likelihood Value	Predicted Burnup (GWd/MTU)	Predicted Time Since Irradiation (days)
MURR	$+28.8 \pm 0.6$	1.01 ± 0.02	305 ± 83
NRX	$+24.7 \pm 1.4$	1.03 ± 0.03	213 ± 86
Magnox	$+12.6 \pm 1.6$	0.73 ± 0.02	2 ± 14
PWR (3.4%)	-5.6 ± 3.2	3.93 ± 0.19	1382 ± 102
PWR (4.45%)	-9.2 ± 5.8	$\geq 3.90 \pm < 0.01$	1197 ± 79
PWR (2.35%)	-10.2 ± 4.9	3.04 ± 0.15	1162 ± 105
PHWR	-24.5 ± 11.5	0.95 ± 0.02	274 ± 88
HFIR	-170 ± 22	$4.40 \pm < 0.01$	1790 ± 79
FBR	$(-1.54 \pm 0.21) \times 10^5$	$\geq 4.73 \pm < 0.01$	0 ± 0

performed using weapons usable plutonium samples produced via two experimental irradiation campaigns [3,4]. Gamma and mass spectrometry was performed on both experimentally irradiated samples in order to obtain measured values for the intra-element isotope ratios employed by the maximum likelihood analysis. Measured values of nine intra-element isotope ratios were obtained for the material which was experimentally irradiated at HFIR, and measured values of eight intra-element isotope ratios were obtained for the material which was experimentally irradiated at MURR.

The results of the maximum likelihood analysis for the measured HFIR irradiated material, which underwent a complex irradiation due to the Gd depletion and significantly changing neutron flux, showed that the reactor-type discrimination methodology correctly identified the HFIR model as the source reactor type. The maximum log-likelihood value for the HFIR model was 17.7 ± 5.0 compared to a maximum possible log-likelihood value of 28.7. The predicted burnup was within 2% of the known burnup of 4.36 ± 0.28 GWd/MTU, and the predicted time since irradiation was within 15% of the known 1601 days of decay.

The results of the maximum likelihood analysis for the measured MURR irradiated material showed that the reactor-type discrimination methodology correctly identified the MURR model as the source reactor type. The maximum log-likelihood value for the MURR model was 29.5 ± 1.1 compared to a maximum possible log-likelihood value of 29.8. The predicted burnup was within 4% of the known burnup of 0.97 ± 0.03 GWd/MTU, and the predicted time since irradiation was within 5% of the known 318 days of decay.

A parametric bootstrap approach was employed to investigate the effects of random errors in the measured intra-element isotope ratio values, and estimate the expected variation in the predicted burnup and time since irradiation values. The estimated variances in the maximum log-likelihood values from the parametric bootstrap approach were smaller than that estimated using the propagation of errors approach on the log-likelihood equation. This supports the use of the maximum log-likelihood equation and associated approximate standard deviation in the log-likelihood equation as a reasonable way to compare reactor models within the reactor library.

In conclusion, the reactor-type discrimination methodology and maximum likelihood analysis works very well for identifying the most likely source reactor model, given the source reactor is contained within the reactor library. The methodology also works very well for predicting the burnup and time since irradiation of the measured material when a likely reactor is identified. For both experimental irradiation cases the full set of ten intra-element isotope ratios was not measurable. Nevertheless, the methodology performed as expected for both cases, identifying the source reactor model and predicting the parameters of burnup and time since irradiation. The two experimental irradiation cases included variations in the fuel sample enrichment, neutron flux shape and magnitude, level of sample burnup, and level of time since irradiation. The study presented here serves to experimentally validate the developed nuclear forensics reactor-type discrimination methodology.

Conflicts of interest

The authors declare there are no conflicts of interest.

Acknowledgements

The majority of the funding for this work (>95%) including the irradiation campaigns, computational efforts, and maximum likelihood analysis was supported by the U.S. Department of Homeland Security, Domestic Nuclear Detection Office under Grant Award Numbers: NSF Grant No. ECCS-1140018, DHS-2012-DN-077-ARI1057-02&03, and DHS-2015-DN-077-ARI1099. The views and conclusions contained in this document are those of the authors and should not be interpreted as necessarily representing the official policies, either expressed or implied, of the U.S. Department of Homeland Security.

A small portion of the funding (<5%) for this work including mass spectrometry sample aliquot preparation and mass spectrometry analysis was supported by the U.S. Department of Energy National Nuclear Security Administration through the Nuclear

Science and Security Consortium under Award Number(s) DE-NA0003180 and/or DE-NA0000979. This report was prepared as an account of work sponsored by an agency of the United States Government. Neither the United States Government nor any agency thereof, nor any of their employees, makes any warranty, express or implied, or assumes any legal liability or responsibility for the accuracy, completeness, or usefulness of any information, apparatus, product, or process disclosed, or represents that its use would not infringe privately owned rights. Reference herein to any specific commercial product, process, or service by trade name, trademark, manufacturer, or otherwise does not necessarily constitute or imply its endorsement, recommendation, or favoring by the United States Government or any agency thereof. The views and opinions of authors expressed herein do not necessarily state or reflect those of the United States Government or any agency thereof.

Appendix A. Supplementary data

Supplementary data to this article can be found online at https://doi.org/10.1016/j.net.2018.11.003.

References

[1] United States Department of Defense, Nuclear Posture Review, 2018.
[2] J.M. Osborn, E.D. Kitcher, J.D. Burns, C.M. Folden III, S.S. Chirayath, Nuclear forensics methodology for reactor-type Attribution of chemically separated plutonium, Nucl. Tech. 201 (2018) 1–10, https://doi.org/10.1080/00295450.2017.1401442.
[3] M.W. Swinney, C.M. Folden III, R. Ellis, S.S. Chirayath, Experimental and computational forensics characterization of weapons-grade plutonium produced in a fast reactor neutron environment, Nucl. Technol. 197 (2017) 1–11, https://doi.org/10.13182/NT16-76.
[4] J.M. Osborn, K.J. Glennon, E.D. Kitcher, J.D. Burns, C.M. Folden III, S.S. Chirayath, Computational and experimental forensics characterization of weapons-grade plutonium produced in a thermal neutron environment, Nucl. Eng. Technol. 50 (2018) 820–828, https://doi.org/10.1016/j.net.2018.04.017.
[5] M. Benedict, T.H. Pigford, H.W. Levi, Nuclear Chemical Engineering, second ed., McGraw-Hill Series in Nuclear Engineering, New York, 1981.
[6] P.M. Mendoza, S.S. Chirayath, C.M. Folden III, Fission product decontamination factors for plutonium separated by PUREX from low-burnup, fast-neutron irradiated depleted UO_2, Appl. Radiat. Isot. 118 (2016) 38–42, https://doi.org/10.1016/j.apradiso.2016.08.021.
[7] T.L. Burr, W.S. Charlton, C.W. Nakhleh, Assessing confidence in inferring reactor type and fuel burnup: a Markov chain Monte Carlo approach, Nucl. Instrum. Methods 555 (2005) 426–434, https://doi.org/10.1016/j.nima.2005.09.041.
[8] D.B. Pelowitz, MCNPX User's Manual, Version 2.7.0, LA-CP-11-00438, Los Alamos National Laboratory, 2011.
[9] D.B. Pelowitz, MCNP6 User's Manual, Version 1.0, LA-CP-13-00634, Los Alamos National Laboratory, 2013.
[10] J. Hendricks, et al., MCNPX 2.6.0 Extensions, LA-UR-08-2216, Los Alamos National Laboratory, Los Alamos, NM, 2008.
[11] N. Xoubi, R.T. Prim III, Modeling of the High Flux Isotope Reactor Cycle 400, Oak Ridge National Laboratory, 2005. ORNL/TM-2004/251.
[12] Missouri University Research Reactor (MURR), Safety Analysis Report, 2006. MU Project # 000763, https://www.nrc.gov/docs/ML0921/ML092110573.pdf.
[13] Westinghouse Electric Company LLC, AP1000 European Design Control Document, 4.3, Cranberry Township, Pennsylvania, 2009.
[14] S.C. Chetal, V. Balasubramaniyan, P. Chellapandi, P. Mohanakrishnan, P. Puthiyavinayagam, C.P. Pillai, S. Raghupathy, T.K. Shanmugham, C.S. Pillai, The design of the prototype fast breeder reactor, Nucl. Eng. Des. 236 (2006) 852–860, https://doi.org/10.1016/j.nucengdes.2005.09.025.
[15] S.S. Chirayath, G. Hollenbeck, J. Ragusa, P. Nelson, Neutronic and nonproliferation characteristics of (PuO_2-UO_2) and (PuO_2-ThO_2) as fast reactor fuels, Nucl. Eng. Des. 239 (2009) 1916–1924, https://doi.org/10.1016/j.nucengdes.2009.05.019.
[16] S.S. Chirayath, J.M. Osborn, T.M. Coles, Trace fission product ratios for nuclear forensics attribution of weapons-grade plutonium from fast and thermal reactors, Sci. Global Secur. 23 (2015) 48–67, https://doi.org/10.1080/08929882.2015.996079.
[17] First Atomic Energy of Canada Limited, Canada Enters the Nuclear Age: a Technical History of Atomic Energy of Canada Limited as Seen from its Research Laboratories, McGill-Queen's Press, Montreal, 1997.
[18] S.E. Jensen, E. Nonbol, Description of the Magnox Type of Gas Cooled Reactor (MAGNOX), NKS/RAK-2(97)TR-c5, Riso National Laboratory, 1998.
[19] S.S. Bajaj, A.R. Gore, The indian PHWR, Nucl. Eng. Des. 236 (2006) 701–722, https://doi.org/10.1016/j.nucengdes.2005.09.028.
[20] A. Ahmad, A. Glaser, A conversion proposal for Iran's IR-40 reactor with reduced plutonium production, Sci. Global Secur. 23 (2015) 3–19, https://doi.org/10.1080/08929882.2015.996074.
[21] R.S. Kemp, Two methods for converting a heavy-water research reactor to use low-enriched-uranium fuel to improve proliferation resistance after startup, Energy Technology & Policy 2 (2015) 39–46, https://doi.org/10.1080/23317000.2015.1012687.
[22] C. Braun, S. Hecker, C. Lawrence, P. Papadiamantis, North Korean Nuclear Facilities after the Agreed Framework, Center for International Security and Cooperation, Stanford University, 2016.
[23] E. Rauch, Development of a Safeguards Approach for a Small Graphite Moderated Reactor and Associated Fuel Cycle Facilities, M.S. Thesis Texas A&M University, 2009.
[24] N.N. Greenwood, A. Earnshaw, Chemistry of the Elements, second ed., Elsevier, Oxford, 1997.
[25] B. Efron, Bootstrap methods: another look at the jackknife, Ann. Stat. 7 (1979) 1–26.